CEBAF Program Advisory Committee Six (PAC6) Proposal Cover Sheet

This proposal must be received by close of business on April 5, 1993 at:

CEBAF
User Liaison Office
12000 Jefferson Avenue
Newport News, VA 23606

Proposal Title

NUCLEON STRUCTURE STUDY BY VIRTUAL COMPTON SCATTERING

Contact Person

Name: BERTIN Pierre-Yves
Institution: IN2P3
Address: L.P.C. Université Clermont II
Address: UNIVERSITÉ BLAISE PASCAL
City, State ZIP/Country: F-63170 AUBIÈRE FRANCE
Phone: (33) 73 40 72 76 **FAX:** (33) 73 26 45 98
E-Mail → BITnet: BERTIN at FRCPN11 **Internet:**

If this proposal is based on a previously submitted proposal or letter-of-intent, give the number, title and date:

CEBAF Use Only

Receipt Date: 4/5/93 (recd 5/27/93 updated version) Log Number Assigned: PR 93-050

By: gp

Nucleon structure study by Virtual Compton Scattering

G. Audit, M. Bernheim, G. Fournier, T. Gousset, P.A.M. Guichon, N. D'Hose, F. Kunne, L. Lakehal-Ayat, C. Marchand, J. Marroncle, J. Mougey, B. Saghai, P. Vernin

DAPNIA/SPhN CE Saclay, France

J. Berthot, P. Bertin, V. Breton, H. Fonvieille

LPC, Clermont II, Aubière, France

J. van de Wiele

IPN Orsay, France

D. Ryckbosh, R. van de Vyver

Nucl. Phys. Lab., B9000 Gent, Belgium

C. Hyde-Wright

Un. of Washington, Seattle, WA 98195, USA

Z.E. Meziani, D. Kawall

Stanford Univ., Stanford, Ca94305, USA

L. Elouadrhiri

Un. of Massachusetts at Amherst, Dpt of Phys. and Astr., Amherst, MA-01003 USA

& THE HALL A COLLABORATION

Abstract

We propose to study nucleon structure by virtual Compton scattering using the Hall A HRS spectrometers. We plan to measure this reaction in the Roper resonance region and at the highest center of mass energy to observe the beginning of the hard scattering regime.

Spokepersons: P. Bertin, G. Fournier.
Contact person: P. Bertin.
Note that the above collaboration list is preliminary and not closed.

I Introduction

One of the basic problems which remains unsolved is the structure of nucleons in term of quarks and gluons. Despite many efforts the non perturbative structure of QCD has not yet been understood and it is clear that new experimental data are needed to guide the theoretical approaches, to exclude some scenarios or to constrain the models.

To be useful, the output of the experiment must be amenable to a simple interpretation in term of the elementary degrees of freedom. This is why pure electromagnetic processes are privileged tools since they can be interpreted directly in terms of the currents carried by the quarks.

In this respect, Virtual Compton Scattering (VCS, see Fig. 1) is a potentially powerful tool to access the nucleon structure. It is the natural complement of form factors, real Compton scattering and deep inelastic scattering.

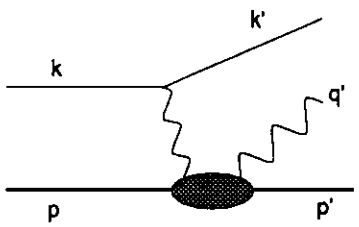

Figure 1 Virtual Compton scattering. The electrons (respectively nucleons and photons) momenta are k, k' (respectively p, p' and q, q')

No data exist up to now for this process. Only real Compton scattering has been investigated so far, at Bonn [1] and Tokyo [2,3] in the resonance region, and Cornell [4,5] and SLAC [6,7] in the deep inelastic region. In the resonance region, differential cross sections have been measured at photon center of mass angles between 40° and 160° at momentum transfers t < 1 GeV and transverse momenta p_T < 0.5 GeV/c. They indicate a strong forward peaking of the Compton cross section. The data at higher energies obtained at p_T < 1 GeV/c are summarized in figure 2 and show an approximate scaling : $s^6 d\sigma/dt$, consistent with quark counting rules. The t dependence is exponential at small t, but flattens out at CM angles above 90°.

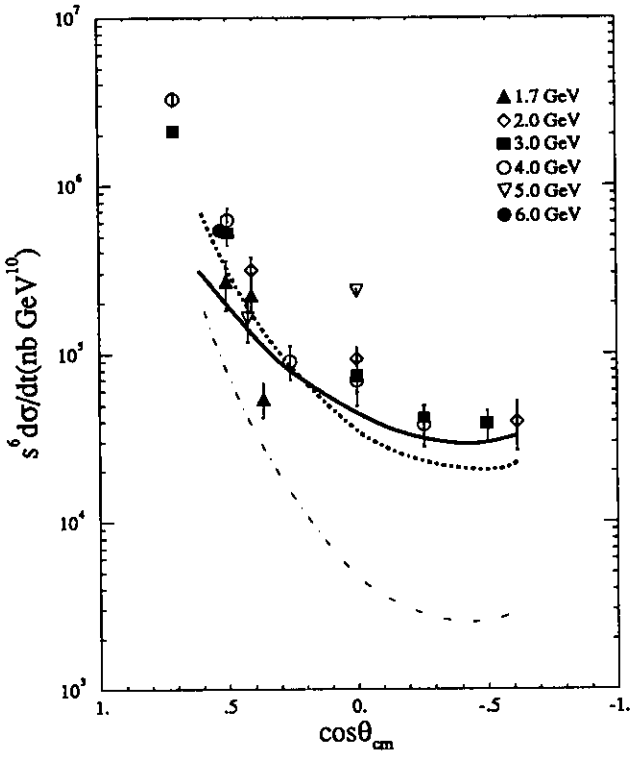

Figure 2 Real Compton scattering. Data are from refs [4,5]. The curve are the di-quark model predictions of ref [20] for a laboratory photon energy of 4 GeV (solid) and 10.2 GeV (dotted)

We propose to investigate the feasibility of the virgin field of VCS at CEBAF using the hall A HRS spectrometers. We aim at studying VCS in two different kinematical regims. First we will study the reaction in the region of the Roper excitation, which will provide a new insight about this not well understood resonance. Second we will perform an exploration of the hard scattering regime at large photon angle and maximum center of mass energy. In this region the short distance approximation begins to make sense [18] and the experiment will provide new and severe tests of the di-quark model predictions. However, in our view this second part of the program can only be exploratory for the following reasons:

At large $Q^2 = -q_\mu q^\mu$ ($Q^2 \gtrsim 2$ GeV^2) and not too small $x_B = Q^2/2p.q$ ($x_B \gtrsim 0.6$) the reaction is dominated by the 3 valence quarks components of the nucleon wave function. This is an important simplification with respect to real photons. However, by contrast with the elastic case, the high Q^2 does not guarantee a small transverse size as long as nothing prevents soft gluon bremsstrahlung (followed by hadronization) by the struck quark. To inhibit this process, which is strongly peaked in the direction of the quark, one has to force the transverse momentum p_T of the produced particle to be larger than the transverse momenta available in the nucleon, that is ~ 0.6 GeV. In our case, the maximum transverse momentum of the final photon is

$$p_T^{max} = \left(s - M^2\right)/2\sqrt{s} \tag{1}$$

with $\sqrt{s}$ the cm energy of the virtual photon and nucleon. For instance $p_T^{max} = 1$ GeV corresponds to $s = 6\,\mathrm{GeV}^2$, above the resonance region for which CEBAF initial energy has been chosen. Thus

the hard scattering region is at the upper limit of CEBAF initial capabilities and it explains why we propose only an exploratory program in this regime.

At this time the theoretical landscape of VCS is almost empty. There exists only one prediction [8] based on asymptotic QCD which is certainly not testable at CEBAF. This may look as an unfavorable situation to make a proposal but we think that it is not bad that experiment be ahead of theory because this often trigger the theoretical activity. Moreover the theoretical interest for VCS is already growing since several calculations based on the di-quark model are underway [9,10]. They will probably be ready for the PAC of June 1993. So the theoretical desert is not a real worry.

It is worth mentioning that this program will also serve as a demonstration of CEBAF unique capabilities. This is illustrated by the comparison of Fig. 3a and Fig. 3b. On Fig. 3a the existing data [11] for the reaction p(e,e'p)X are plotted versus the invariant missing mass. Clearly the photon cannot be distinguished from the π^o. The simulation of our proposed experiment shown in Figure 3b (see section 3.C) clearly indicates that, thanks to the excellent energy resolution, this separation will be possible at CEBAF, thereby allowing VCS experiments without photon detection.

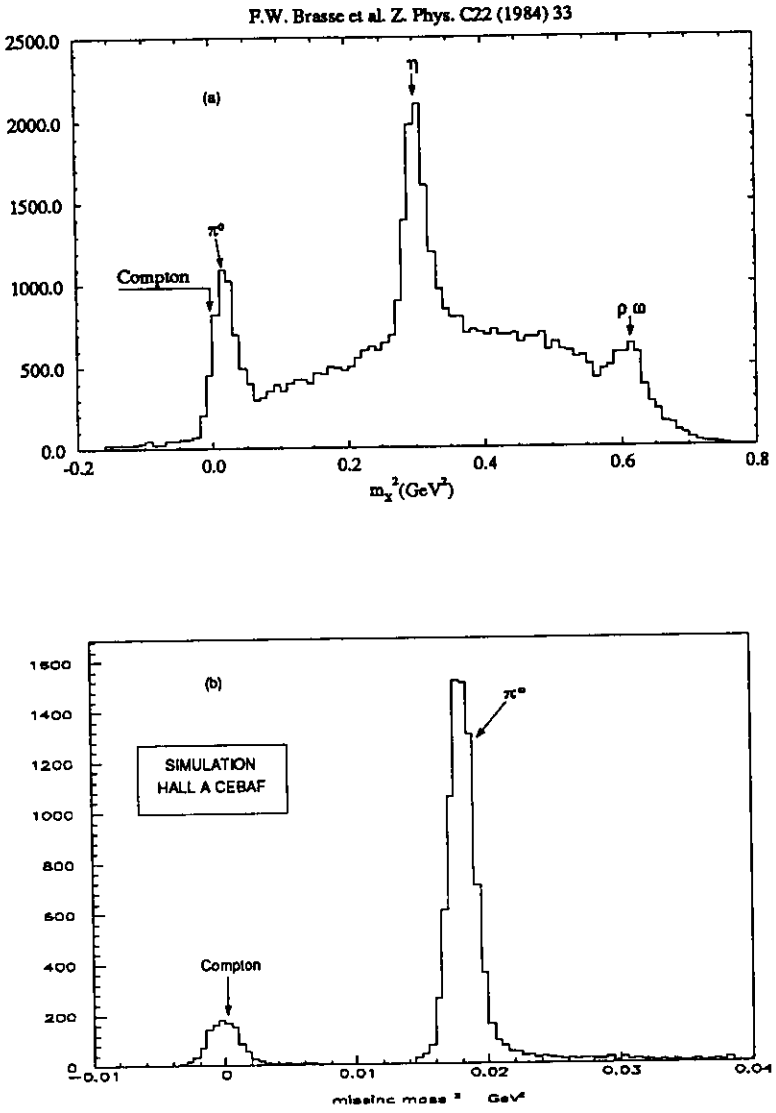

Figure 3 Missing mass squared spectrum for the reaction p(e,e'p)X.

II Theoretical aspects and program presentation

The experiment will actually measure the cross section for exclusive electroproduction of a real photon. To lowest order in $\alpha \sim 1/137$ the process is described by the coherent sum of the amplitudes shown in Fig.4. In the following, γ^* or γ^v will denote the virtual photon *of the VCS process.* We note $\theta^{\gamma^*\gamma}$ the angle between γ^* and the real photon. Our convention is that the azimuthal angle of the latter is $\phi = 0^o$ when it is emitted in the same half plane as the scatterred electron.

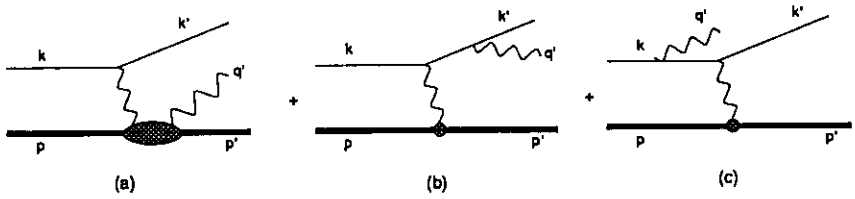

Figure 4 Electroproduction of a real photon. a: Virtual Compton Scattering. b,c: Bethe Heitler process.

VCS refers to amplitude (a) while (b,c) describe the Bethe-Heitler (BH) process which is exactly calculable from QED provided the elastic form factors G_M and G_E are known. This is the case in the energy range of CEBAF. As is well known the BH process is strongly peaked along the electron lines. This allows to define regions for the final photon where BH is either dominant, either negligible, or of the same order of magnitude as VCS, in which case they interfere. This is illustrated on Fig.5.

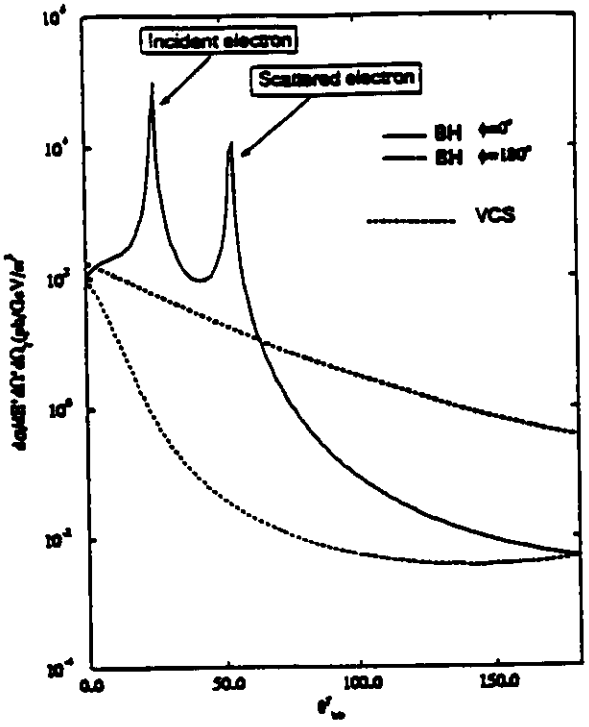

Figure 5 Bethe-Heider and VCS (as estimated by eq. 15) cross sections. ϕ is the azimuthal angle of the final photon with respect to the electrons plane.

The interference between VCS and BH can yield valuable information about the real to imaginary ratio of the VCS amplitude. We will make a tentative exploration of the interference region but we think that to get quantitative results one needs out of plane experiments which we postpone until the first phase of the program has been achieved. Thus most of the measurements will be performed in the regions where BH is negligible before VCS.

We have computed the amplitude of BH without any approximation and checked our results with respect to the results of Mo and Tsai [12]. Our way to estimate the cross section for VCS is presented in the next section. Since we choose kinematics mostly where VCS and BH do not interfere, we have added incoherently the cross sections of (a) and (b+c) to evalnate the counting rates.

In the rest of this section we discuss only the VCS amplitude. To lowest order in α the amplitude is defined by (helicity labels are omitted for simplicity):

$$T_{VCS} = \int d^4x\, e^{i(q+q')\cdot x/2} < p'|T(J_\mu(x/2)J_\nu(-x/2))|p > \epsilon'^{\mu}(q')\epsilon^{\nu}(q) \qquad (2)$$

with $T(...)$ the time ordering operator, ϵ the polarization vectors of the photons and J_μ the electromagnetic current of the proton which in term of quark fields reads

$$J_\mu = \sum_{\text{flavors}} e_f \overline{\psi}\gamma_\mu\psi, \quad e_u = (2/3)e, \ldots \qquad (3)$$

This amplitude depends on 3 independent invariants. The usual choices are

$$Q^2 = -q_\mu q^\mu, \;\; s = (p+q)^2, \;\; t = \left(q - q'\right)^2 \qquad (4)$$
$$Q^2, \;\; x_B = \frac{Q^2}{2p.q} = \frac{Q^2}{Q^2 + s - M^2}, \;\; t.$$

It is often convenient to use θ^γ_{cm} the c.m. angle of the photons, instead of t because the transverse momentum of the real photon is simply

$$|p_T| = \frac{s - M^2}{2\sqrt{s}} \sin\theta^\gamma_{cm}. \qquad (5)$$

Equation 2 displays the physical information of VCS. That the amplitude can be written directly in terms of currents is the advantage of a pure electromagnetic process. Its actual evaluation depends strongly on the kinematical domain.

Resonance region

In the resonance region, the process is essentially soft due to the small transverse momentum of the photon and therefore long ranged effects associated with confinement dominate the dynamics. We are in the domain of low energy effective models, like for instance constituent quark model, bag models, Skyrmions, etc...

We shall focus on the Roper region ($\sqrt{s} \sim 1.45\,\mathrm{GeV}$) because this resonance is a brick wall for all the models. The point is that it has the same parity as the nucleon but stands below the first negative parity state. This is difficult to explain in a simple quark model unless one introduce *ad hoc* distortions in the potential [13]. On the other hand the bag model, as well as solitons models, can interpret this anomaly in term of a breathing mode of the surface [15,16,14]. However this collective effect is difficult to master from the theoretical point of view due to the non linear coupling between the quark motion and surface (or soliton) vibrations. Drastic approximations are necessary to produce the Roper excitation and one can only conclude that these model have the potential to explain this resonance.

On the experimental side the bulk of experimental data concerns pion nucleon scattering and pion photoproduction [17]. In both cases the interpretation is complicated by the final or initial state interaction. A pure electromagnetic process like VCS will provide a cleaner information about the resonance itself.

We shall first perform an angular distribution in the region where BH is negligible at $Q^2 = 2\,\mathrm{GeV}^2$ (see next section for the details). Then we shall focus on the backward region in order to measure the cross section at $\theta^\gamma_{cm} = 180^\circ$ with a longitudinal-transverse separation. The motivation is that this allows a separate measurement of helicity conserving and helicity non conserving cross sections. The argument goes as follows:

Let λ, λ' the helicities of the virtual and real photon and λ_p, λ'_p the helicities of the initial and final proton. Then, due to total angular momentum conservation, we have:

$$\lambda - \lambda_p = -\lambda' + \lambda'_p \qquad (6)$$

If the virtual photon is longitudinal ($\lambda = 0$) and since the real photon is transverse ($\lambda' = \pm 1$) we have

$$\lambda'_p + \lambda_p = \pm 1 \tag{7}$$

which implies $\lambda'_p = \lambda_p$.

If the virtual photon is transverse then

$$\lambda'_p + \lambda_p = 0, \pm 2 \tag{8}$$

and the only solution is $\lambda'_p = -\lambda_p$.

Thus the longitudinal part of the cross section contains only the helicity conserving amplitudes and vice versa for the transverse part. This measurement will be performed as a function of Q^2 in the region of the Roper resonance (see next section and table 2) and as a function of θ^{γ}_{cm} (table 3). This information on helicity conserving and non conserving amplitude will yield new tests of the models for this resonance at non zero Q^2.

Hard region

In the hard region, the reaction depends essentially on the small distance structure of the nucleon, the long distance effects manifesting themselves only through the probability amplitude (distribution amplitude) that the 3 quarks be at the same point or more exactly in a transverse distance of order $1/Q$. This is the spirit of the factorization scheme. The rest of the reaction is calculated perturbatively via minimum gluon exchange [18]. However at CEBAF energy this description does not apply because the maximum transverse momentum of the photon is not that large. Several authors [19,20] have proposed that such semi hard reaction can be treated in the framework of the di–quark model. The factorization scheme is the same as before but two quarks are replaced by a phenomenological object called the di-quarks with form factors which describe non perturbative correlations. Such models are rather successful for real Compton scattering (see Fig. 2, even at modest energy ($s \sim 6\,\mathrm{GeV}^2$) so it is worth testing their predictions in the case of VCS. We do not conceal that the maximum value of s which can be reached by the initial phase of CEBAF is somewhat low ($s \sim 4\,\mathrm{GeV}^2$) but the virtuality of the photon puts us in a more favorable situation.

We propose to extend the longitudinal-transverse separation at fixed $Q^2 = 1\ GeV^2$ from the resonance region into this semi-hard regime (table 4), and to perform an angular distribution at $s \sim 4\,\mathrm{GeV}^2$ up to the highest possible transverse momenta (table 5).

III Experimental Aspects

A. Method

We propose to investigate VCS at CEBAF by detecting the scattered electron and the proton in coincidence in the HRS spectrometers of hall A. From the measured 4–momenta P_e and P_p and the incident beam energy E_i, we reconstruct the missing mass M_X:

$$M_X^2 = E_X^2 - \vec{P}_X^2$$

where,

$$E_X = E_i + M - E_e - E_p$$
$$\vec{P}_X = \vec{P}_i - \vec{P}_e - \vec{P}_p. \tag{9}$$

Then the VCS events are characterized by the photon mass, $M_X = 0$. As is visible from figure 3, the good resolution of the HRS spectrometers allows a clean separation of VCS and π^0 events, and no detection of the photon is needed. On the contrary, previous real Compton scattering experiments needed to detect the scattered photon, because the poor knowledge of the incident photon energy and angle ($\theta \sim 1/\gamma$) prevented any separation by missing mass criteria. Although the HRS have small solid angles, the Lorentz boost (see Figure 6) helps to focus the protons in a small cone around the virtual photon. Indeed the Jacobian $d\cos\theta_{p'}/d\cos\theta_{\gamma'}$ is about 1/20 , and thus a large phase space for the real photon is sampled. This helps to keep the counting rates at a reasonnable level.

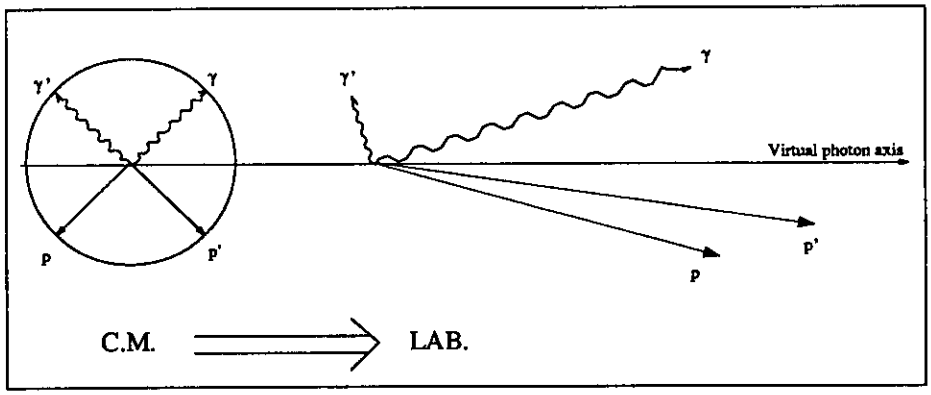

Figure 6 CM to laboratory system Lorentz transformation for the final photon and proton, at two cm photon angles (resp. γ, p and γ', p')

B. Apparatus

Spectrometers

We will make use of the two spectrometers of hall A in their standard configuration as described in the Table 4.1 of ref. [21]. Standard electron and proton identification will be used.

Targets

Thanks to CEBAF high duty cycle, we are not limited by accidental (e',p) coincidence rates, nor by single rates (< 0.5 MHz) and we will use therefore a luminosity of $10^{38}\ cm^{-2}s^{-1}$. This corresponds to 40 μA beam current on a 10 cm long liquid hydrogen target, and we will therefore use the high power cryogenic target developed for the hall A. Its specifications can be found in table 8.3 of the ref. [21]. No modification of the vacuum target chamber is required.

C. Simulation of the experiment

In this section, we present and justify our hypotheses for estimating the counting rates.

VCS cross section evaluation

The cross section of VCS, when the BH amplitude is negligible, can be written as [22]:

$$\frac{d^5\sigma}{dP_{e'}d\Omega_{e'}dtd\phi} = \Gamma(E_i, P_{e'}, \theta_{e'})2\pi\frac{d^2\sigma(s,Q^2,t)}{dtd\phi} \tag{10}$$

where Γ is the virtual photon flux factor and $d^2\sigma(s,Q^2,t)/dt\,d\phi$ the cross section of photoproduction by virtual photon. We have:

$$\Gamma(E_i, P_{e'}, \theta_{e'}) = \frac{\alpha}{2\pi^2}.\frac{E'}{E_i}.\frac{(W^2-M^2)}{2M}.\frac{1}{Q^2}.\frac{1}{(1-\epsilon)} \tag{11}$$

$$\epsilon = \frac{1.}{(1+2\frac{Q^2+(E_i-E')^2}{Q^2}.tg^2(\frac{\theta_{e'}}{2}))} \tag{12}$$

$$\frac{d^2\sigma(s,Q^2,t)}{dtd\phi} = \frac{d\sigma_T}{dtd\phi} + \epsilon\frac{d\sigma_L}{dtd\phi} + \epsilon\frac{d\sigma_{TT}}{dtd\phi}\cos(2\phi) + \sqrt{\epsilon(1+\epsilon)}\frac{d\sigma_{LT}}{dtd\phi}\cos(\phi) \tag{13}$$

The counting rates that we give for VCS, in absence of any experimental result, are estimated from the real Compton scattering data (Figure 2 and ref.[5]), according to the following approximations:

1. Only the transverse part is taken into account:

$$d\sigma_L = 0,\ d\sigma_{TL} = 0,\ d\sigma_{TT} = 0 \tag{14}$$

   This strong assumption, which gives conservative counting rates, is supported by 2 facts:

   - In the deep inelastic region, the ratio $R = \sigma_L/\sigma_T$ is small, $0.1 \sim 0.2$.
   - In the electroproduction of pion the longitudinal part of the cross section is important only at low value of quadritransfert $|t| < .3GeV^2$ and the interference part σ_{TT} and σ_{TL} are always small [22].

2. We neglect any dependence in $\cos\theta^{\gamma}_{cm}$ for the VCS cross section. The value of the cross section $d\sigma_T/dt$ is taken at $\theta^{\gamma}_{cm} = 90^0$, angle between the scattered and virtual photon, where experimentally the cross section of real Compton seems to be minimum (Figure 2). Thus our estimate is conservative.
3. The dependance in s is taken as a scaling in s^{-6}. This is roughly satisfied by real Compton scattering in our energy range (figure 2).
4. No dependence on Q^2 is assumed for the virtual cross section which is taken equal to the value at $Q^2 = 0$.

$Q^2(\mathrm{GeV}^2)$	$2\pi s^6 d\sigma/dtd\phi(\mu\mathrm{b\,GeV}^{10})$
.1	92.
.5	36.
1.	13.
2.	2.6
3.	.8

Table 1 Prediction for the transverse cross section of VCS at $s = 2.356\ \mathrm{GeV}^2$, using the data of [11] on the S_{11} and D_{13} resonance.

In summary, we have taken:

$$2\pi s^6 \frac{d\sigma_T(Q^2,s,t)}{dtd\phi} = 30\mu b.GeV^{10} \tag{15}$$

Check of our evaluation

To verify that our estimate at $Q^2 \neq 0$ is correct, we checked it at $s = 2.356\,GeV^2$ where the electroproduction of the resonances S_{11} and D_{13} have been well measured [11]. We assume that the VCS cross section is dominated by the excitation of the two resonances multiplied by the branching ratio of decay of the resonance in gamma and proton.

$$\frac{d\sigma}{d\cos\theta_{cm}d\phi} = \frac{1.}{4\pi}(\sigma_T^{S11}(Q^2).Br(S11 \to p+\gamma) + \sigma_T^{D13}(Q^2).Br(D13 \to p+\gamma)) \tag{16}$$

The parametrization of the result of F.W. Brasse et al. [11] is given by

$$\sigma_T^{S11}(Q^2) = 21.6\ e^{-.385.Q^2}\ \mu b \quad \text{and} \quad \sigma_T^{d13}(Q^2) = 127.4\ e^{-1.6.Q^2}\ \mu b \tag{17}$$

$$Br(S11 \to p+\gamma) = (0.15 \pm .05)\% \quad \text{and} \quad Br(D13 \to p+\gamma) = (0.5 \pm 0.5)\% \tag{18}$$

The results of our estimation are given in table 1 for the sum of S11 and D13 contributions. The absolute values of the cross section at small Q^2 are in agreement with our evaluation (eq. 15). The resonances form factors produces a fast decrease in Q^2 but this is mostly cancelled by the non resonant background which has a weak Q^2 dependence. This is why we neglect any Q^2 dependence in our counting rate estimation.

π^0 electroproduction cross section

The physical backgrounds we have to consider when detecting VCS by missing mass reconstruction are the reactions with one electron and one proton which can be accepted by the apparatus. The closest one to VCS in missing mass is the electroproduction of neutral pions:

$$e + P \to e' + P + \pi^0.$$

(Of course, as a by product of the VCS measurement, we will also obtain the corresponding data on π^0 production, which is an interesting reaction per se).

We give now a rough estimate of the π^0 counting rate. We distinguish 2 cases:

1. $|t| \gg 0$ *and* $|u| \gg 0$

The π^0 transverse cross section is computed under two assumptions:

- The π^0 cross section and the π^+ cross section are in the ratio 1:2 following a prediction of O. Nachtman [23]. This leads to the prediction:

$$\frac{d\sigma_T}{dt}(\gamma^v p \to \pi^+ n) : \frac{d\sigma_T}{dt}(\gamma^v p \to \pi^o p) : \cdots$$
$$\frac{d\sigma_T}{dt}(\gamma^v n \to \pi^o n) : \frac{d\sigma_T}{dt}(\gamma^v n \to \pi^- p) = 8 : 4 : 1 : 2 \tag{19}$$

- The transverse cross section of $\gamma^v p \to \pi^+ n$ is given by:

$$2\pi . \frac{d\sigma_T}{dt d\phi} = \frac{19.6}{(W^2 - M^2)^2} e^{(1.2t)} \ \mu b . GeV^{-2} \tag{20}$$

This empirical parametrization given by ref. [22] works from Q^2=0 to Q^2=3.3 GeV^2 and W arround 2 and 3 GeV.

2. $|t| \gg 0$ and $|u| \sim 0$
From R.L. Anderson et al [6] for the backward π^0 production we have taken a cross section which scales with s^{-3} and with a dependence on u given by $e^{1.5u}$. We normalize the cross section from the data at $E_\gamma = 5\ GeV$ according to:

$$2\pi \frac{d\sigma}{du d\phi} = \frac{28\ e^{1.5u}}{s^3} \mu b / GeV^{-8} \tag{21}$$

We have given no dependence in Q^2. In this way we conservatively maximize the production rate.

Single counting rates

– Electron

The counting rate of single electron takes into account:

- The elastic cross section on the proton.
- The electroproduction of the $\Delta(1.232)$ and of two resonances at $\sqrt{s}$ = 1.5 and 1.7 GeV.
- The deep inelastic cross section.

– Proton

The proton counting rate is dominated by photoproduction reactions. We estimate it using the CELEG code [25] with a flux of quasireal photon given by the equivalent radiation length. In CELEG we have allowed for the excitation of all the N^* and Δ resonances.

– Accidental coincidences

From the single rates in each arm, we compute rates for accidental coincidences with the following assumptions:

- Electrons and protons are fully identified, and all the others are rejected.
- The time coincidences peak between the two arms has a full width of 2 nanoseconds.
- We require the two particles to originate from the same point in the target (spatial coincidence) within $\pm 2\sigma$ resolution. The transverse resolution for each spectrometer is 1mm FWHM (table A.4.1 of [21]), and we assume that the spectrometers see an effective target length of 100 mm.

These timing and spatial requirements ensure a very low level of accidental coincidences (tables 2 to 5).

Backgrounds

– Target windows

Due to the excellent vertex resolution described above, the unwanted target window contamination can be rejected easily. This is mandatory to be able to detect the small VCS cross sections.

– Deuterium contamination

The hydrogen used for the experiment may contain some small percentage of deuterium but this is not a major problem. Indeed, though (e,e'p) events on deuterium with high initial proton momenta may fall in the acceptance of the spectrometers, they are easily identified at missing energies of 2.2 MeV if we use $M_{target} = M_{deuterium}$.

Experimental resolution

We have estimated the expected experimental resolution on the missing mass squared M_X^2 in two way: one using the results of Monte Carlo simulation which we use to determine the acceptance, and the other by differentiation of the equation $M_X^2 = 0$.. In tables 2 to 5, we give the resolving power $m_{\pi^0}^2/\sigma(M_X^2)$ which appears to be always larger than 10, allowing thus a clean separation between VCS and π^0 events.

Phase space acceptance

In order to determine the acceptance of the two spectrometers, we have simulated the experiment by a Monte Carlo code, using the specifications of ref. [21] on angular and momentum resolutions and acceptances. Radiative corrections have been taken into account by allowing the incident and scattered electrons to radiate a photon. The angular peaking approximation and the equivalent radiator for internal bremsstrahlung have been used [12].

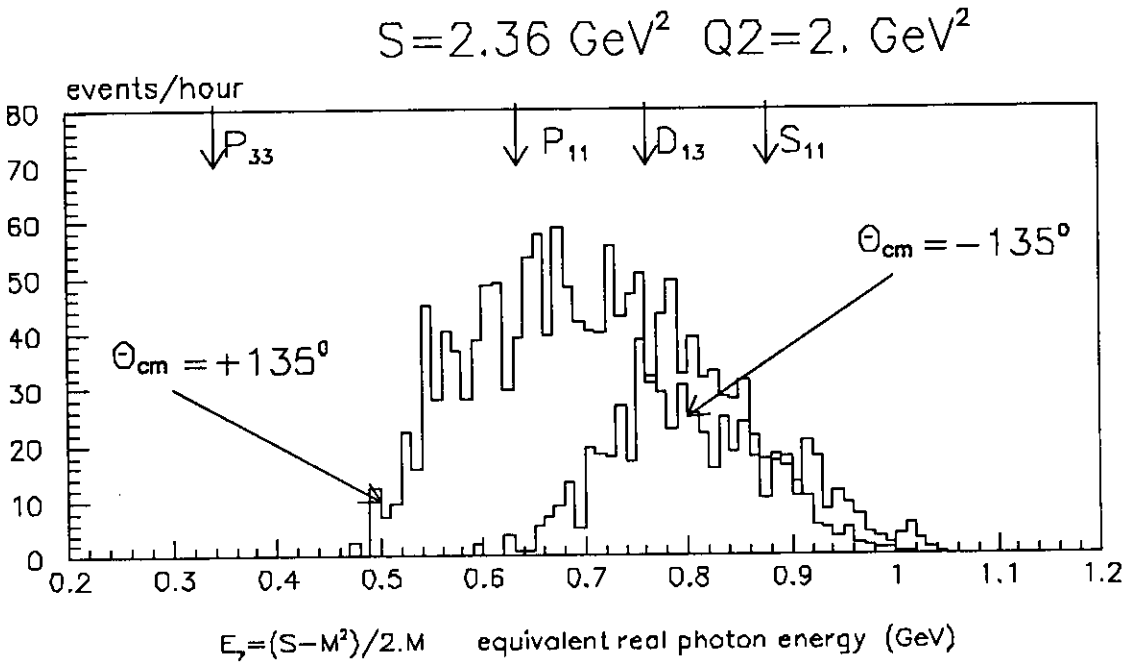

Figure 7 Acceptance as a function of the equivalent photon energy, for two kinematics of table 3.

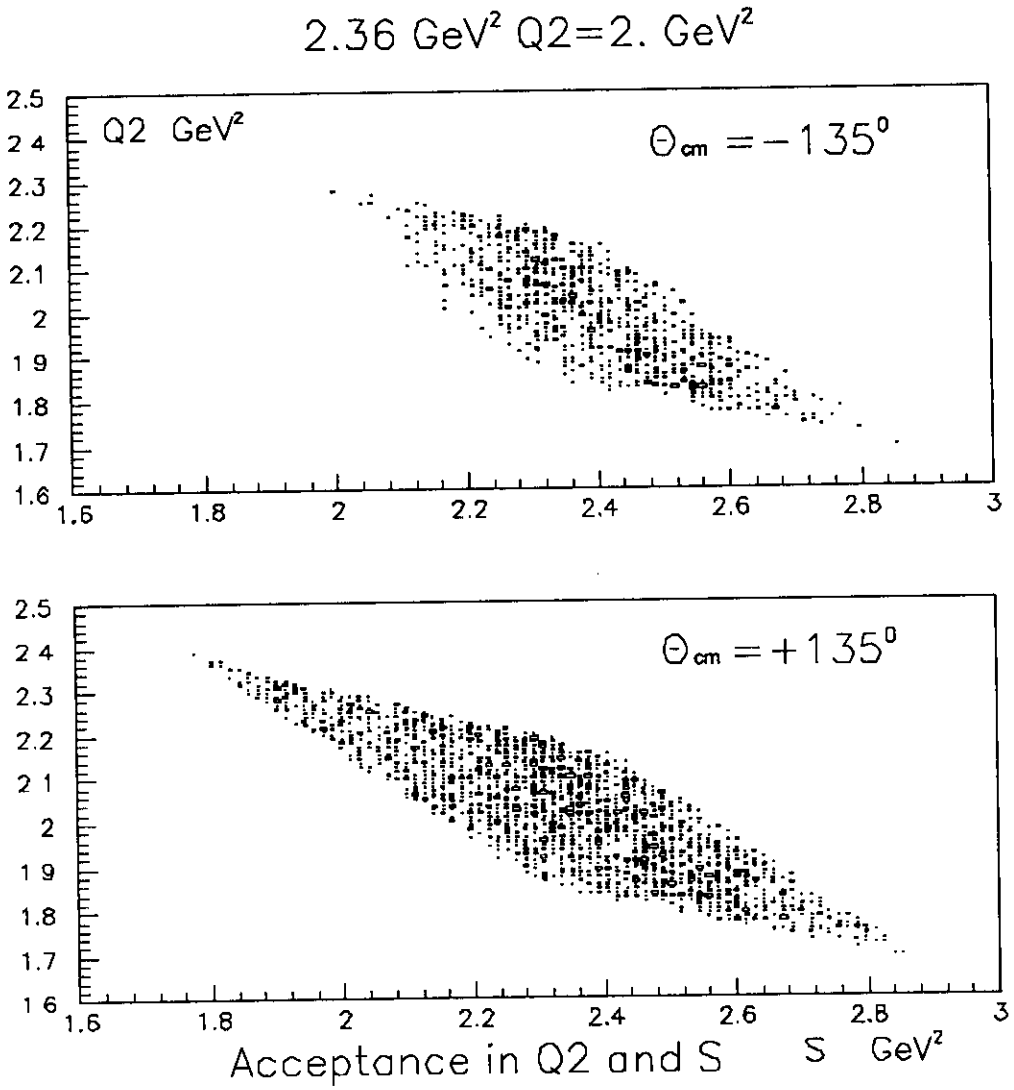

Figure 8 Combined acceptance of the apparatus in Q^2 and s

Figure 7 shows the acceptance in s for two kinematics where the proton is detected on both sides of the virtual photon. The acceptance in s is wide, and allow us to cover the range of P_{11} S_{11} and D_{13}. Figure 8 shows the shape of the acceptance for the same kinematic on a two dimensional scatter plot s/Q^2: the range of Q^2 covered with one spectrometer setting is quite extended.

D. Choice of kinematics for the proposed study

The choice of the kinematics was conditionned by the following points:

- The incident energy of the beam is less than 4 GeV. Some points labeled " ** " in tables 2 and 4 need 6 GeV of incident energy, but they are only shown as an illustration of what we could gain at higher energy. (No beam time is requested at 6 GeV.)
- The spectrometers are used in the standard configuration. The minimum scattering angle of 12.5^0 severely limits the range of experimental investigation.
- We restrict to kinematics where the Bethe-Heitler process is negligible before VCS, except one kinematic in the angular distribution (θ^{γ}_{cm} near 90°).
- For the tranverse-longitudinal separation at $\theta^{cm} = 180^0$ we make the balance between the counting rate at low ϵ and the necessity to have the two ϵ very different. We try to have at least $\epsilon_a - \epsilon_b > 0.3$.
- In the resonance region, we choose to center s at 2.36 GeV^2 on the S_{11} where electroproduction data [11] give us a control on the counting rates.

Resonance region

Due to the limitations described above, we can perform the transverse longitudinal (T/L) separation at $\theta^{\gamma}_{cm} = 180^0$ in the resonance region ($s = 2.36$ GeV^2) at quadritransfers Q^2 of the virtual photon between .2 and 3.5 GeV^2 (table 2). In order to get a reasonable determination of the longitudinal contribution, we require more than 1000 counts for each setting.

The angular distribution at $s = 2.36\ GeV^2$ is presented in table 3. The angular limitation is due to the requirement that the BH amplitude be negligible before the Compton amplitude. We perform this measurement at the same θ_{cm} angles at $\phi = 0^0$ and $\phi = 180^0$. For this kinematic, we require 10^4 counts in order to keep opened the possibility of a separation between the T, L, TT and TL cross sections. We point out that at ($\theta_{cm} = 135^0$, $\phi = 0^0$) the BH process is of the same order (1/3) of magnitude than the VCS. This will allow us to explore the BH-VCS interference. This will be useful to prepare the next generation of experiment.

Hard region

The transverse longitudinal (T/L) separation at $\theta^{\gamma}_{cm} = 180^0$ and $Q^2 = 1$ GeV^2 will be extended from $s = 2GeV^2$ to $s = 4GeV^2$ (table 4). For the last points ($4a, 4b$) at the largest s, counting rates are low and we require only a few hundred counts.

At the highest possible value of s (4 GeV^2) and at $Q^2 = 1$ GeV^2, we intent to perform an angular distribution so as to explore the beginning of the hard scattering region (table 5). The maximum transverse momentum p_T will be 0.7 GeV.

E. Beam time request

We resume the beam time requirement in table 6. We need 430 hours for a first exploration of Virtual Compton Scattering. Including the running time for the tests, we request 20 days of beam in the hall A, at maximum energy of 4 GeV and 40 μA beam current.

IV Bibliography

1. M.Jung et al., Z. Phys. C10 (1981) 197
2. Y. Wada et al., Nucl. Phys. B247 (1984) 313
3. T. Ishii et al, Nucl. Phys. B254 (1985) 458
4. J. Deutsch et al., Phys. Rev. D8 (1973) 3828
5. M.A. Shupe et al. Phys. Rev. D19 (1979) 1929
6. R.L. Anderson et al., Phys. Rev. Lett. 25 (1970)1218
7. D.O. Caldwell et al., Phys.Rev. Lett. 33 (1974) 868
8. G. Farrar et H. Zhang, Phys. Rev. D41 (1990) 3348
9. T. Gousset, work in progress
10. M Schürmann, work in progress
11. F.W. Brasse et al., Z. Phys. C22 (1984) 33
12. L.W. Mo and Y.S. Tsai, Rev. Mod. phys. 41 (1969) 205
13. N. Isgur and G. Karl, Phys. Rev. D19 (1979) 2653
14. T. de Grand and C. Rebbi, Phys. Rev. D9 (1978)2358
15. P.A.M. Guichon, Phys. Lett. B164 (1985) 361
16. J.D. Breit, Nucl. Phys. B202 (1982) 147
17. F. Foster and G. Hughes, Rep. Prog. Phys. 46 (1983) 1445
18. S. Brodsky, in Perturbative Quantum Chromodynamics, A.H. Mueller editor, World Scientific (1989)
19. S. Frederiksson, in Di-quarks, M. Anselmino and E. Predazzi editors, World Scientific (1988)
20. P. Kroll, M. Schürmann and W. Schweïger, Nucl. Phys. Int. J. Mod. Phys. A6 (1991) 4107
21. Conceptual Design Report, CEBAF, April 1990
22. P. Brauel et al., Z. Phys. C3 (1979) 101
23. O. Nachtman, Nucl. Phys. B115 (1976) 61
24. R.L. Anderson et al., Phys. Rev. 14 (1976) 679
25. D. Joyce, "CELEG", Users Manual CLAS Notes 89004 (1988)

	s GeV^2	Q2 GeV^2	ϵ	E_i GeV	θ_e degrees	P_e GeV	θ_p degrees	P_p GeV	θ_ν degrees	θ_γ degrees	P_γ GeV
1a	2.36	0.20	0.89	2.55	12.50	1.65	-20.97	1.26	-20.97	159.0	0.26
1b	2.36	0.20	0.50	1.30	36.16	0.40	-13.67	1.26	-13.67	166.3	0.26
2a	2.36	0.50	0.93	3.82	12.50	2.76	-28.09	1.50	-28.09	151.9	0.23
2b	2.36	0.50	0.45	1.52	49.58	0.47	-16.26	1.50	-16.26	163.7	0.23
3a	2.36	1.00	0.89	4.00	17.57	2.68	-29.21	1.85	-29.21	150.8	0.19
3b	2.36	1.00	0.50	2.04	46.63	0.72	-19.06	1.85	-19.06	160.9	0.19
4a	2.36	2.00	0.76	4.00	27.94	2.15	-25.53	2.48	-25.53	154.5	0.14
4b	2.36	2.00	0.35	2.53	65.74	0.67	-15.23	2.48	-15.23	164.8	0.14
5a	2.36	3.00	0.59	4.00	39.87	1.61	-20.52	3.07	-20.52	159.5	0.12
5b	2.36	3.00	0.30	3.11	70.87	0.72	-13.30	3.07	-13.30	166.7	0.12
6a	2.36	3.50	0.49	4.00	47.55	1.35	-17.81	3.35	-17.81	162.2	0.11
6b	2.36	3.50	0.30	3.43	69.66	0.78	-13.03	3.35	-13.03	167.0	0.11
**7a	2.36	4.00	0.74	6.00	26.90	3.08	-23.19	3.64	-23.19	156.8	0.10
7b	2.36	4.00	0.35	3.90	61.52	0.98	-14.09	3.64	-14.09	165.9	0.10

	θ^γ_{cm} degrees	s GeV^2	t GeV^2	u GeV^2	$X_{Bjo.}$	P_t GeV	$N_{Comp.}$ c/h	N_{Beth} c/h	N_e c/s	N_p c/s	Acci. c/h	$\frac{m^2_\pi}{\sigma(M^2_\pi)}$
1a	180.	2.36	-1.19	0.39	0.12	0.00	$2.47\ 10^5$	$2.03\ 10^0$	$2.93\ 10^5$	$1.81\ 10^5$	33.2	63.2
1b	180.	2.36	-1.19	0.39	0.12	0.00	$9.81\ 10^3$	$0.61\ 10^0$	$7.91\ 10^3$	$1.14\ 10^5$	0.4	130.7
2a	180.	2.36	-1.55	0.45	0.25	0.00	$3.52\ 10^5$	$2.06\ 10^0$	$1.83\ 10^5$	$6.43\ 10^4$	8.9	39.8
2b	180.	2.36	-1.55	0.45	0.25	0.00	$7.06\ 10^3$	$0.44\ 10^0$	$1.79\ 10^3$	$3.85\ 10^4$	0.0	119.5
3a	180.	2.36	-2.13	0.53	0.40	0.00	$2.84\ 10^5$	$1.22\ 10^0$	$2.57\ 10^4$	$1.48\ 10^4$	0.3	44.2
3b	180.	2.36	-2.13	0.53	0.40	0.00	$1.27\ 10^4$	$0.40\ 10^0$	$8.29\ 10^2$	$3.99\ 10^3$	0.0	103.3
4a	180.	2.36	-3.21	0.61	0.57	0.00	$1.49\ 10^5$	$0.48\ 10^0$	$1.72\ 10^3$	$1.93\ 10^3$	0.0	63.2
4b	180.	2.36	-3.21	0.61	0.57	0.00	$8.23\ 10^3$	$0.16\ 10^0$	$9.98\ 10^1$	$9.72\ 10^2$	0.0	113.4
5a	180.	2.36	-4.26	0.66	0.67	0.00	$7.07\ 10^4$	$0.32\ 10^0$	$2.18\ 10^2$	$2.39\ 10^3$	0.0	85.2
5b	180.	2.36	-4.26	0.66	0.67	0.00	$9.96\ 10^3$	$0.10\ 10^0$	$3.30\ 10^1$	$2.39\ 10^3$	0.0	116.0
6a	180.	2.36	-4.78	0.68	0.70	0.00	$4.35\ 10^4$	$0.19\ 10^0$	$8.43\ 10^1$	$2.62\ 10^3$	0.0	96.6
6b	180.	2.36	-4.78	0.68	0.70	0.00	$1.24\ 10^4$	$0.10\ 10^0$	$2.43\ 10^1$	$2.62\ 10^3$	0.0	115.6
**7a	180.	2.36	-5.29	0.69	0.73	0.00	$3.18\ 10^3$	$0.31\ 10^0$	$4.20\ 10^2$	$1.72\ 10^4$	0.0	65.9
7b	180.	2.36	-5.29	0.69	0.73	0.00	$1.99\ 10^2$	$0.13\ 10^0$	$2.60\ 10^1$	$2.84\ 10^3$	0.0	110.8

Table 2: Invariants, p_t and counting rates at S=2.36 GeV^2 and $\theta^\gamma_{cm} = 180^0$.
L/T separation of VCS in the resonance region as a function of Q^2.

	s GeV^2	Q2 GeV^2	ε	E_i GeV	θ_e degrees	P_e GeV	θ_p degrees	P_p GeV	θ_γ degrees	θ_γ degrees	P_γ GeV
1	2.36	2.00	0.76	4.00	27.94	2.15	-12.50	1.98	-25.53	-73.47	0.60
2	2.36	2.00	0.76	4.00	27.94	2.15	-16.81	2.25	-25.53	-97.32	0.36
3	2.36	2.00	0.76	4.00	27.94	2.15	-19.70	2.37	-25.53	-121.95	0.24
4	2.36	2.00	0.76	4.00	27.94	2.15	-22.61	2.45	-25.53	-158.11	0.17
5	2.36	2.00	0.76	4.00	27.94	2.15	-25.53	2.48	-25.53	154.50	0.14
6	2.36	2.00	0.76	4.00	27.94	2.15	-28.45	2.45	-25.53	107.05	0.17
7	2.36	2.00	0.76	4.00	27.94	2.15	-31.36	2.37	-25.53	70.89	0.24
8	2.36	2.00	0.76	4.00	27.94	2.15	-34.25	2.25	-25.53	46.26	0.36

	θ^γ_{cm} degrees	s GeV^2	t GeV^2	u GeV^2	$X_{Bjo.}$	P_t GeV	$N_{Comp.}$ c/h	N_{Bath} c/h	N_e c/s	N_p c/s	Acci. c/h	$\frac{m_\pi^2}{\sigma(M_\pi^2)}$
1	-112.0	2.36	-2.35	-0.25	0.57	-0.45	$3.89\ 10^2$	$2.98\ 10^0$	$1.72\ 10^3$	$1.35\ 10^5$	0.46	11.4
2	-135.0	2.36	-2.81	0.21	0.57	-0.34	$5.34\ 10^2$	$0.99\ 10^0$	$1.72\ 10^3$	$3.31\ 10^4$	0.07	18.3
3	-150.0	2.36	-3.02	0.43	0.57	-0.24	$8.79\ 10^2$	$0.50\ 10^0$	$1.72\ 10^3$	$3.50\ 10^4$	0.04	29.
4	-165.0	2.36	-3.16	0.56	0.57	-0.12	$1.19\ 10^3$	$0.51\ 10^0$	$1.72\ 10^3$	$2.10\ 10^4$	0.02	54.
5	180.	2.36	-3.21	0.61	0.57	0.00	$1.49\ 10^3$	$0.48\ 10^0$	$1.72\ 10^3$	$1.93\ 10^3$	0.0	63.
6	+165.0	2.36	-3.16	0.56	0.57	0.12	$1.63\ 10^3$	$1.41\ 10^0$	$1.72\ 10^3$	$1.91\ 10^3$	0.00	39.5
7	+150.0	2.36	-3.02	0.43	0.57	0.24	$1.55\ 10^3$	$1.62\ 10^1$	$1.72\ 10^3$	$3.79\ 10^3$	0.00	28.4
8	+135.0	2.36	-2.81	0.21	0.57	0.34	$1.47\ 10^3$	$5.22\ 10^2$	$1.72\ 10^3$	$3.59\ 10^3$	0.00	23.

Table 3: Invariants, p_t and counting rates at $Q2 = 2.\ GeV^2$ and $S = 2.36\ GeV^2$.
Angular distribution of VCS in the resonance region.

	s GeV^2	Q2 GeV^2	ε	E_i GeV	θ_e degrees	P_e GeV	θ_p degrees	P_p GeV	θ_ω degrees	θ_γ degrees	P_γ GeV
1a	2.00	1.00	0.91	4.00	16.97	2.87	-33.74	1.67	-33.74	146.3	0.16
1b	2.00	1.00	0.40	1.66	64.65	0.53	-18.42	1.67	-18.42	161.6	0.16
2a	2.36	1.00	0.89	4.00	17.57	2.68	-29.21	1.85	-29.21	150.8	0.19
2b	2.36	1.00	0.50	2.04	48.63	0.72	-19.08	1.85	-19.08	160.9	0.19
3a	3.00	1.00	0.83	4.00	18.83	2.34	-22.87	2.17	-22.87	157.1	0.23
3b	3.00	1.00	0.40	2.26	50.82	0.80	-13.87	2.17	-13.87	166.1	0.23
4a	4.00	1.00	0.71	4.00	21.45	1.80	-15.88	2.69	-15.88	164.1	0.28
4b	4.00	1.00	0.49	4.00	34.03	0.93	-12.50	2.69	-12.50	167.5	0.28
**5a	5.00	1.00	0.82	6.00	12.96	3.27	-14.63	3.22	-14.63	165.4	0.31
5b	5.00	1.00	0.67	4.61	15.97	1.88	-12.513	3.22	-12.51	167.4	0.31

	θ^γ_{cm} degres	u GeV^2	t GeV^2	u GeV^2	$X_{Bjo.}$	P_t GeV	$N_{Comp.}$ c/h	N_{Both} c/h	N_e c/s	N_p c/s	Acci. c/h	$\frac{m^2_\pi}{\sigma(M^2_\pi)}$
1a	180.	2.00	-1.83	0.59	0.47	0.00	$7.14\ 10^{3}$	$3.80\ 10^{0}$	$1.76\ 10^{4}$	$4.08\ 10^{4}$	0.5	49.2
1b	180.	2.00	-1.83	0.59	0.47	0.00	$1.41\ 10^{2}$	$0.90\ 10^{0}$	$2.14\ 10^{2}$	$1.51\ 10^{4}$	0.0	141.6
2a	180.	2.36	-2.13	0.53	0.40	0.00	$2.84\ 10^{3}$	$1.22\ 10^{0}$	$2.57\ 10^{4}$	$1.48\ 10^{4}$	0.3	44.2
2b	180.	2.36	-2.13	0.53	0.40	0.00	$1.27\ 10^{2}$	$0.40\ 10^{0}$	$8.29\ 10^{2}$	$3.99\ 10^{3}$	0.0	32.4
3a	180.	3.00	-2.68	0.44	0.32	0.00	$7.24\ 10^{2}$	$0.30\ 10^{0}$	$1.76\ 10^{4}$	$2.80\ 10^{4}$	0.3	42.6
3b	180.	3.00	-2.68	0.44	0.32	0.00	$2.49\ 10^{1}$	$0.67\ 10^{-1}$	$5.60\ 10^{2}$	$8.68\ 10^{3}$	0.0	81.6
4a	180.	4.00	-3.59	0.35	0.24	0.00	$1.01\ 10^{2}$	$0.42\ 10^{-1}$	$6.69\ 10^{3}$	$2.10\ 10^{3}$	0.0	41.5
4b	180.	4.00	-3.59	0.35	0.24	0.00	$1.60\ 10^{1}$	$0.23\ 10^{-1}$	$1.27\ 10^{3}$	$2.10\ 10^{3}$	0.0	53.3
**5a	180.	5.00	-4.53	0.29	0.20	0.00	$1.43\ 10^{2}$	$0.24\ 10^{-1}$	$3.13\ 10^{4}$	$2.51\ 10^{3}$	0.0	26.5
5b	180.	5.00	-4.53	0.29	0.20	0.00	$3.56\ 10^{1}$	$0.15\ 10^{-1}$	$7.14\ 10^{3}$	$2.51\ 10^{3}$	0.0	35.0

Table 4: Invariants, p_t and counting rates at Q2=1. GeV^2 and $\theta^\gamma_{cm} = 180.^0$.
L/T separation of VCS at fixed Q^2 as a fonction of c.m. energy s.

	s GeV^2	Q2 GeV^2	x	E_i GeV	θ_e degres	P_e GeV	θ_p degres	P_p GeV	θ_ν degres	θ_γ degres	P_γ GeV
1	4.00	1.00	0.71	4.00	21.45	1.80	-15.88	2.69	-15.88	-195.88	0.28
2	4.00	1.00	0.71	4.00	21.45	1.80	-20.23	2.66	-15.88	124.01	0.31
3	4.00	1.00	0.71	4.00	21.45	1.80	-24.64	2.56	-15.88	90.90	0.41
4	4.00	1.00	0.71	4.00	21.45	1.80	-29.16	2.40	-15.88	66.21	0.56
5	4.00	1.00	0.71	4.00	21.45	1.80	-33.84	2.19	-15.88	48.10	0.75

	θ^γ_{cm} degres	s GeV^2	t GeV^2	u GeV^2	$X_{Bjo.}$	P_t GeV	$N_{Comp.}$ c/h	N_{Both} c/h	N_e c/s	N_p c/s	Acci. c/h	$\frac{m^2_\pi}{\sigma(M^2_\pi)}$
1	180.0	4.00	-3.59	0.35	0.24	0.00	$8.40\ 10^1$	$0.44\ 10^{-1}$	$6.69\ 10^3$	$2.10\ 10^3$	0.01	41.51
2	165.0	4.00	-3.53	0.29	0.24	0.20	$1.01\ 10^2$	$0.94\ 10^{-1}$	$6.69\ 10^3$	$2.07\ 10^3$	0.01	24.01
3	150.0	4.00	-3.36	0.12	0.24	0.39	$8.57\ 10^1$	$0.61\ 10^0$	$6.69\ 10^3$	$2.20\ 10^3$	0.16	16.04
4	135.0	4.00	-3.07	-0.16	0.24	0.55	$7.85\ 10^1$	$4.49\ 10^0$	$6.69\ 10^3$	$3.84\ 10^3$	0.03	12.61
5	120.0	4.00	-2.71	-0.53	0.24	0.68	$7.81\ 10^1$	$2.78\ 10^1$	$6.69\ 10^3$	$9.39\ 10^3$	0.09	10.99

Table 5: Invariants, p_t and counting rates at S=4. GeV^2
Angular distribution at hight transverse momenta p_t.

T/L at $S = 2.36\ GeV^2$ and $\theta^{\gamma}_{cm} = 180^0$	1a & 1b 20 h	2a & 2b 20 h	3a & 3b –	4a & 4b 20 h	5a & 5b 20 h	6a & 6b 20 h			100 h
$S = 2.36$, $Q2 = 2.\ GeV^2$ angular distr.	1 20 h	2 20 h	3 20 h	4 15 h	5 –	6 15 h	7 10 h	8 10 h	110 h
T/L at $Q2 = 1.\ GeV^2$ and $\theta^{\gamma}_{cm} = 180^0$	1a & 1b 20 h	2a & 2b 20 h	3a & 3b 40 h	4a & 4b 60 h					140 h
$S = 4.$, $Q2 = 1.\ GeV^2$ angular distr.	1 –	2 20 h	3 20 h	4 20 h	5 20 h				80 h
Total beam times									430 h

Table 6: Beam time requirement.